ISSN 0021-8944, Journal of Applied Mechanics and Technical Physics, 2024, Vol. 65, No. 3, pp. 456–464. © Pleiades Publishing, Ltd., 2024.
Russian Text © J. Dutta.

EVOLUTION OF THE MATHEMATICAL MODEL CHARACTERIZING THE THERMAL FIELD DEVELOPED IN SUBMERGED ARC WELDING

J. Dutta[1,*]

UDC 621.791.011

Abstract: A two-dimensional exact analytical solution of the thermal field developed during the submerged arc welding process with visualization of the thermal surface contour for analyzing the heat flow in the domain with the hybrid application of Duhamel's theorem and finite integral transform approach is obtained. The thermal field arising in submerged arc welding of thick EH36 steel plates is studied. An ellipsoidal heat source model is assumed. The developed thermal field is investigated with variations of several process parameters, such as the heat source velocity, heat input, and lag time of movement of the heat source involved in the welding process.

Keywords: integral transform, Duhamel's theorem, thermal field, submerged arc welding, EH36 steel.

DOI: 10.1134/S0021894424030076

INTRODUCTION

The use of thick-walled steel plates is very common in industrial manufacturing. The main areas of application include the oil, gas and chemical industries. Other important fields of application are wind energy and shipbuilding. The EH36 steel is a high-tensile-strength steel utilized in various shipbuilding applications [1]. The prediction of the temperature history of the welded components has a significant impact on the thermal stress, distortion, residual stresses, and, more importantly, on the fatigue behavior of the welded structures [2].

Submerged arc welding is extensively used in industries where thick steel sheets or plates are involved or where long welds are recommended. The process comprises forming of a welded joint between steel components by using an electric arc submerged beneath a layer of the granular flux [3].

Biswas et al. [4] conducted an experimental thermo-mechanical study of submerged arc welded double-sided fillet joints and validated the same with a finite element method based analysis. Ghosh et al. [5] developed an analytical model for the transient temperature distribution during submerged arc welding for joining two steel plates. Ghosh and Chattopadhyay [6] mathematically modelled the thermal field in the submerged arc welding process. Birsan et al. [7] developed a 3D finite element method based simulation model of heat transfer in the submerged double arc welding process for steel pipe joints. Sudnik et al. [8] numerically and experimentally presented a non-stationary heat source to identify the physics behind the submerged arc welding process. Podder et al. [9] produced a numerical solution of a heat transfer model of submerged arc welding in the most generalized way along with experimental validation. Yadav et al. [10] performed experimental observations on mild steel plates to explore the thermal field, characteristics of the weld bead geometry, and microstructure of the heat-affected and fusion zones.

[1]Department of Basic Science and Humanities, St. Thomas' College of Engineering and Technology, Kolkata, India; *jaideep.dutta@mechresearch.net.in. Translated from Prikladnaya Mekhanika i Tekhnicheskaya Fizika, Vol. 65, No. 3, pp. 74–82, May–June, 2024. Original article submitted October 10, 2022; revision submitted June 25, 2023; accepted for publication November 27, 2023.

*Corresponding author.

Till date, very few researchers [5, 6] have attempted to find an analytical solution of the thermal field induced by submerged arc welding. The present research is dedicated to establishing an exact analytical solution of a two-dimensional temperature field developed in the submerged arc welding process of EH36 steel joints. The Gaussian type double-ellipsoidal heat source model is employed.

1. MATHEMATICAL FRAMEWORK

The differential equations and the boundary and initial conditions of the transient problem for a nonstationary temperature field arising in submerged arc welding are presented below, and the method used to solve the problem is described.

1.1. Formulation of the Governing Differential Equations

The following equations of a 2D transient heat transfer model are solved [11]:

$$\frac{\partial^2 T}{\partial x^2} + \frac{\partial^2 T}{\partial y^2} + \frac{Q_g}{k} = \frac{1}{\alpha}\,\frac{\partial T}{\partial t}, \qquad 0 < x < L, \quad 0 < y < L. \tag{1}$$

Here T [°C] is the local temperature, $Q_g(x, y, t)$ is the power of the double-ellipsoidal heat source of the Gaussian type moving in the form of a torch during submerged arc welding [9]

$$Q_g(x, y, t) = \frac{6\sqrt{3}\, f_f Q}{a_f bc\pi^{3/2}} \exp\Big(- \frac{3[x + v(\tau - t)]^2}{a_f^2} - \frac{3y^2}{b^2}\Big), \tag{2}$$

k is the thermal conductivity, α is the thermodiffusion coefficient, L [m] is the domain length in the x direction. f_f is the amount of heat in the frontal quadrant, a_f [m] is the semi-axis length in the x direction, b [m] is the ellipsoid length, c [m] is the ellipsoid width, v [m/s] is the heat source velocity, and τ is lag time of the moving heat source.

To solve Eq. (1), we impose the boundary conditions

$$x = 0: \quad \frac{\partial T}{\partial x} = 0, \qquad x = L: \quad \frac{\partial T}{\partial x} = 0,$$

$$y = 0: \quad \frac{\partial T}{\partial y} = 0, \qquad y = L: \quad \frac{\partial T}{\partial y} = 0$$

and the initial conditions

$$t = 0: \quad T = T_i.$$

In view of Eq. (2), Eq. (1) can be expressed is dimensional variables as

$$\frac{\partial^2 \theta}{\partial X^2} + \frac{\partial^2 \theta}{\partial Y^2} + CQ^* \exp\Big(- \frac{3[X + U(\xi - F)]^2}{A_f^2} - \frac{3Y^2}{B^2}\Big) = \frac{\partial \theta}{\partial F}, \tag{3}$$

where $\theta = (T - T_i)/T_i$, $X = x/L$, $Y = y/L$, $C = 6\sqrt{3}\, f_f/\pi^{3/2}$, $Q^* = QL^2/(ka_f bcT_i)$, $A_f = a_f/L$, $B = b/L$, $F = \alpha t/L^2$, $U = vL/\alpha$, and $\xi = \alpha\tau/L^2$.

1.2. Solution Methodology: Duhamel's Theorem and Finite Integral Transform

By virtue of Duhamel's theorem [11], Eq. (3) reduces to

$$\frac{\partial^2 \bar\theta}{\partial X^2} + \frac{\partial^2 \bar\theta}{\partial Y^2} = \frac{\partial \bar\theta}{\partial F}, \tag{4}$$

where

$$\theta(X, Y, F) = \int\limits_{\bar F = 0}^{F} \bar\theta(X, Y, F; \bar F)\, d\bar F, \tag{5}$$

and the modified initial conditions can be written as

$$\bar\theta\Big|_{(X,Y,F=\bar F)} = CQ^* \exp\Big(- \frac{3[X + U(\xi - \bar F)]^2}{A_f^2} - \frac{3Y^2}{B^2}\Big). \tag{6}$$

Application of the finite cosine integral transform with respect to X [11]

$$\int\limits_{X=0}^{1} \frac{\partial^2\bar{\theta}}{\partial X^2}\cos(m\pi X)\,dX + \int\limits_{X=0}^{1} \frac{\partial^2\bar{\theta}}{\partial Y^2}\cos(m\pi X)\,dX - \int\limits_{X=0}^{1} \frac{\partial\bar{\theta}}{\partial F}\cos(m\pi X)\,dX = 0$$

to Eq. (4) yields

$$-m^2\pi^2\bar{\theta}' + \frac{\partial^2\bar{\theta}'}{\partial Y^2} - \frac{\partial\bar{\theta}'}{\partial F} = 0, \tag{7}$$

where

$$\bar{\theta}'(m,Y,F) = \int\limits_{X=0}^{1} \bar{\theta}(X,Y,F)\cos(m\pi X)\,dX.$$

Similarly, application of the finite integral transform with respect to Y to Eq. (7) yields

$$(m^2\pi^2 + n^2\pi^2)\bar{\theta}'' + \frac{d\bar{\theta}''}{dF} = 0, \qquad m = 0,1,2,3,\ldots, \quad n = 0,1,2,3,\ldots, \tag{8}$$

where

$$\bar{\theta}''(m,n,F) = \int\limits_{Y=0}^{1} \bar{\theta}'(m,Y,F)\cos(n\pi Y)\,dY = \int\limits_{X=0}^{1}\int\limits_{Y=0}^{1} \bar{\theta}(X,Y,F)\cos(m\pi X)\cos(n\pi Y)\,dX\,dY.$$

The solution of Eq. (8) can be written as follows:

$$\bar{\theta}''(m,n,F) = C_{XY}\exp[-(m^2\pi^2 + n^2\pi^2)F]. \tag{9}$$

Application of the inverse finite integral transform to Eq. (9) yields

$$\bar{\theta}(X,Y,F;\bar{F}) = \sum_{m=0}^{\infty}\sum_{n=0}^{\infty} C_{XY}\exp[-(m^2\pi^2 + n^2\pi^2)F]\cos(m\pi X)\cos(n\pi X). \tag{10}$$

With application of the initial condition (6), Eq. (10) yields the relation for the constants C_{XY}:

$$C_{XY}\cos(m\pi X)\cos(n\pi Y) = CQ^*\exp\Big(-\frac{3[X + U(\xi - \bar{F})]^2}{A_f^2} - \frac{3Y^2}{B^2}\Big). \tag{11}$$

Multiplying the left and right sides of equality (11) by $\cos(m\pi X)\cos(n\pi Y)$ and integrating with respect to X and Y, we obtain

$$\int\limits_{X=0}^{1}\int\limits_{Y=0}^{1} C_{XY}\cos^2(m\pi X)\cos^2(n\pi Y)\,dX\,dY =$$

$$= CQ^*\int\limits_{X=0}^{1}\int\limits_{Y=0}^{1}\exp\Big(-\frac{3[X + U(\xi - \bar{F})]^2}{A_f^2} - \frac{3Y^2}{B^2}\Big)\cos(m\pi X)\cos(n\pi Y)\,dX\,dY.$$

From the condition of orthogonality of the functions $\cos(m\pi X)\cos(n\pi Y)$, we find

$$C_{XY} = \frac{\sqrt{\pi}\,A_f}{4\sqrt{3}}\exp\Big(\frac{3\xi^2U^2}{A_f^2} - \pi\xi U + \frac{\pi^2A_f^2}{12}\Big)$$

$$\times\Big\{\exp(2\pi\xi U)\Big[\operatorname{erf}\Big(\frac{6\xi U + \pi A_f^2 + 6}{2\sqrt{3}\,A_f}\Big) - \operatorname{erf}\Big(\frac{6\xi U + \pi A_f^2}{2\sqrt{3}\,A_f}\Big)\Big] +$$

$$+\operatorname{erf}\Big(\frac{6\xi U - \pi A_f^2 + 6}{2\sqrt{3}\,A_f}\Big) - \operatorname{erf}\Big(\frac{6\xi U - \pi A_f^2}{2\sqrt{3}\,A_f}\Big)\Big\}\frac{\sqrt{\pi}\,B\exp(\pi^2B^2/12)}{4\sqrt{3}}$$

$$\times\Big[\operatorname{erf}\Big(\frac{\pi B^2 + 6}{2\sqrt{3}\,B}\Big) - \operatorname{erf}\Big(\frac{\pi B^2 - 6}{2\sqrt{3}}\Big)\Big]\,4CQ^*\exp\Big(-\frac{3U^2(\xi - \bar{F})^2}{A_f^2}\Big). \tag{12}$$

Hence,

$$\bar{\theta}(X,Y,F;\bar{F}) = \sum_{m=0}^{\infty}\sum_{n=0}^{\infty} C_{XY}\exp\left[-(m^2\pi^2+n^2\pi^2)F\right]\cos\left(m\pi X\right)\cos\left(n\pi X\right).$$

In view of Eq. (5), Eq. (12) yields

$$\theta(X,Y,F) = \sum_{m=0}^{\infty}\sum_{n=0}^{\infty}\Big\{4CQ^*M_1M_2\exp\left[-(m^2\pi^2+n^2\pi^2)F\right]$$

$$\times\frac{\sqrt{\pi}\,A_f}{2\sqrt{3}\,U}\Big[\operatorname{erf}\Big(\frac{U\sqrt{3}\,(F-\xi)}{A_f}\Big)+\operatorname{erf}\Big(\frac{U\xi\sqrt{3}}{A_f}\Big)\Big]\cos\left(m\pi X\right)\cos\left(n\pi X\right)\Big\}, \tag{13}$$

where

$$M_1 = \frac{\sqrt{\pi}\,A_f}{4\sqrt{3}}\exp\Big(\frac{3\xi^2U^2}{A_f^2}-\pi\xi U+\frac{\pi^2A_f^2}{12}\Big)$$

$$\times\Big\{\exp\left(2\pi\xi U\right)\Big[\operatorname{erf}\Big(\frac{6\xi U+\pi A_f^2+6}{2\sqrt{3}\,A_f}\Big)-\operatorname{erf}\Big(\frac{6\xi U+\pi A_f^2}{2\sqrt{3}\,A_f}\Big)\Big]$$

$$+\operatorname{erf}\Big(\frac{6\xi U-\pi A_f^2+6}{2\sqrt{3}\,A_f}\Big)-\operatorname{erf}\Big(\frac{6\xi U-\pi A_f^2}{2\sqrt{3}\,A_f}\Big)\Big\},$$

$$M_2 = \frac{\sqrt{\pi}\,B\exp\left(\pi^2B^2/12\right)}{4\sqrt{3}}\Big[\operatorname{erf}\Big(\frac{\pi B^2+6}{2\sqrt{3}\,B}\Big)-\operatorname{erf}\Big(\frac{\pi B^2-6}{2\sqrt{3}\,B}\Big)\Big].$$

The temperature distribution can be obtained from Eq. (13) with application of the inverse Fourier transform. The integrals can be approximated using a quadrature correlation [13], which yields

$$\theta(X,Y,F) = \frac{1}{(2\pi)^2}\sum_{k_x=1}^{\infty}\sum_{k_y=1}^{\infty}\theta_0\exp\left[i(k_xX+k_yY+\omega F)\right], \tag{14}$$

where $k_x = 1,2,3,\ldots$ and $k_y = 1,2,3,\ldots$ are the wave numbers, $\omega = i\alpha(k_x+k_y)^2$, $i=\sqrt{-1}$, and θ_0 is the wave frequency:

$$\theta_0 = 4CQ^*M_1M_2\,\frac{\sqrt{\pi}\,A_f}{2\sqrt{3}\,U}\Big[\operatorname{erf}\Big(\frac{U\sqrt{3}\,(F-\xi)}{A_f}\Big)+\operatorname{erf}\Big(\frac{U\xi\sqrt{3}}{A_f}\Big)\Big].$$

2. RESULTS AND DISCUSSION

Shipbuilding structures are essentially dependent upon application of thick plates, and a EH36 steel plate is one of the common materials used (melting temperature $T_m = 1425^\circ$C, thermal conductivity $k = 52$ W/(m $\cdot\,^\circ$C), density $\rho = 7800$ kg/m^3, and specific heat $C_p = 470$ J/(kg $\cdot\,^\circ$C) [12]). In the present study, we consider the thermal field distribution in a plate 100 mm long and 30 mm thick (Fig. 1).

Podder et al. [9] conducted an experimental investigation of submerged arc welding on mild steel plates. They considered an ellipsoidal heat source (along the x and y axes) [9]), and the process parameters were $Q = 14\,000$ W, $y = 0.025$ m, $x = 0.3$ m, $v = 0.5$ m/min, $f_f = 0.42$, $k = 31.3$ W/(m $\cdot\,^\circ$C), and $\rho = 7850$ kg/m^3.

The experimental [9] temperature curve as a function of time is compared to the present theoretical dependence in Fig. 2. It is seen that the these curves display a similar overall behavior. The peak temperature of the experimental research is 462.28°C, while the present theoretical model predicts 460.88 °C. Both curves display rapid heating and subsequent gradual cooling, which is a typical trend of the $T(t)$ behavior in submerged arc welding [6–8]. There is some difference in the gradients of the curves.

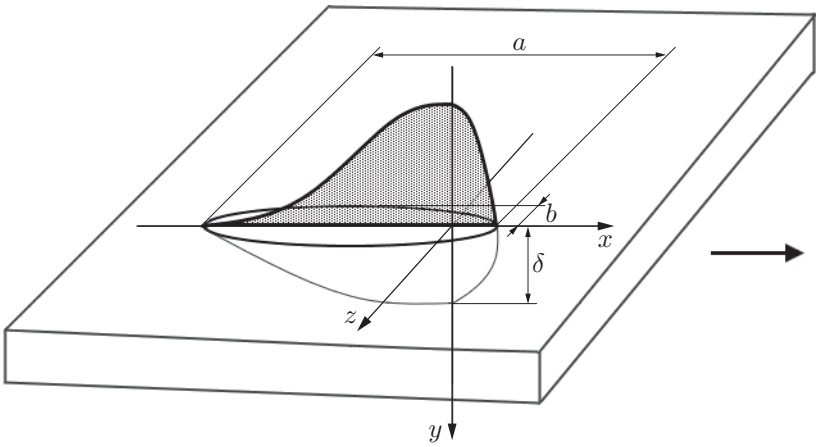

Fig. 1. Schematic diagram of the double ellipsoidal heat source model in a thick plate (the arrow shows the welding direction).

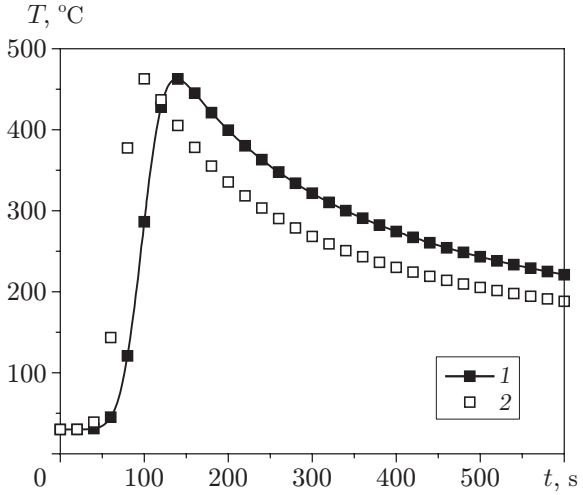

Fig. 2. Time evolution of the temperature obtained theoretically in the present study (*1*) as compared to the experimental data [9] (*2*).

Figure 3 shows the temperature distribution as a function of time for $y = 0.03$ m, $x = 0.01$ m, $v = 0.005$ m/s, $f_f = 0.42$, $k = 52$ W/(m · °C), $\rho = 7850$ kg/m^3, $C_p = 470$ J/(kg · °C), $\tau = 20$ s, $a_f = 0.03$ m, $b = 0.005$ m, $\delta = 0.008$ m, $T_i = 30$ °C, and two values of the heat input Q. It is found that the peak temperature increases with amplification of Q.

Figure 4 demonstrates the temperature distribution curve as a function of time for $y = 0.03$ m, $x = 0.01$ m, $Q = 25\,000$ W, $f_f = 0.42$, $k = 52$ W/(m · °C), $\rho = 7850$ kg/m^3, $C_p = 470$ J/(kg · °C), $\tau = 25$ s, $a_f = 0.03$ m, $b = 0.005$ m, $\delta = 0.008$ m, and two values of the arc motion velocity. As the velocity increases from 0.0045 to 0.0050, the peak temperature decreases. An increase in the moving arc velocity means that the source moves faster over the plate surface. The energy (amount of heat) released on the plate surface decreases in this case.

Figure 5 portrays the temperature distribution as a function of temperature for $y = 0.03$ m, $x = 0.01$ m, $Q = 25\,000$ W, $f_f = 0.42$, $k = 52$ W/(m · °C), $\rho = 7850$ kg/m^3, $C_p = 470$ J/(kg · °C), $v = 0.005$ m/s, $a_f = 0.03$ m, $b = 0.005$ m, $\delta = 0.008$ m, and two values of the lag time of heating τ. It is seen that the temperature decreases as the lag time increases from $\tau = 20$ s to $\tau = 25$ s.

Figure 6 illustrates the temperature variation along the EH36 steel plate for $y = 0.03$ m, $x = 0.01$ m, $Q = 25\,000$ W, $v = 0.005$ m/s, $f_f = 0.42$, $k = 52$ W/(m · °C), $\rho = 7850$ kg/m^3, $C_p = 470$ J/(kg · °C), $a_f = 0.03$ m, $b = 0.005$ m, $\delta = 0.008$ m, $\tau = 20$ s, and various lag times of heating. It is seen that the temperature decreases as

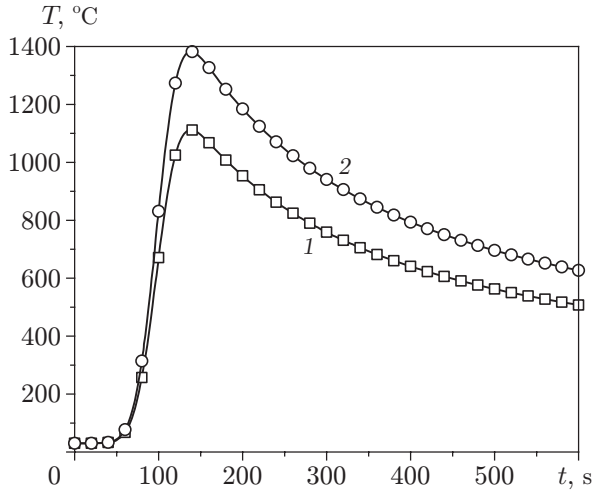

Fig. 3.

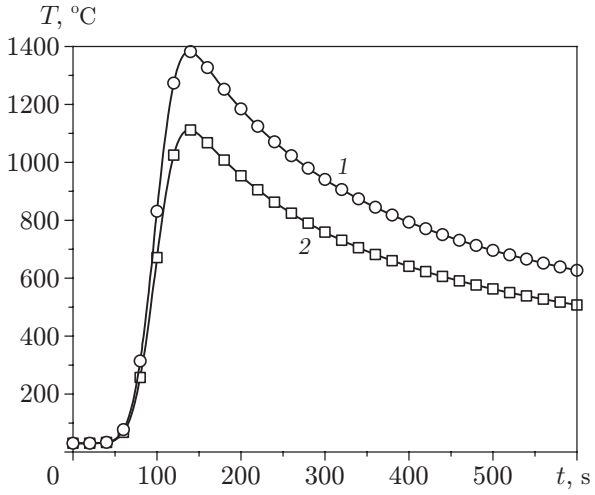

Fig. 4.

Fig. 3. Temperature distributions versus time for various heat input values: $Q = 20\,000$ (*1*) and 25 000 W (*2*).

Fig. 4. Temperature distributions versus time for various arc motion velocities: $v = 0.0045$ (*1*) and 0.0050 m/s (*2*).

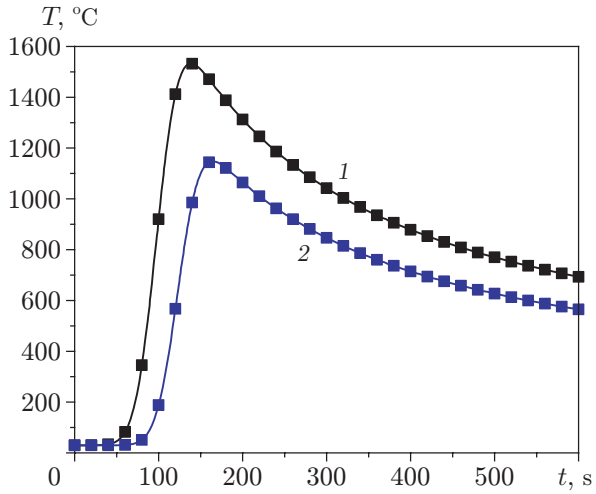

Fig. 5.

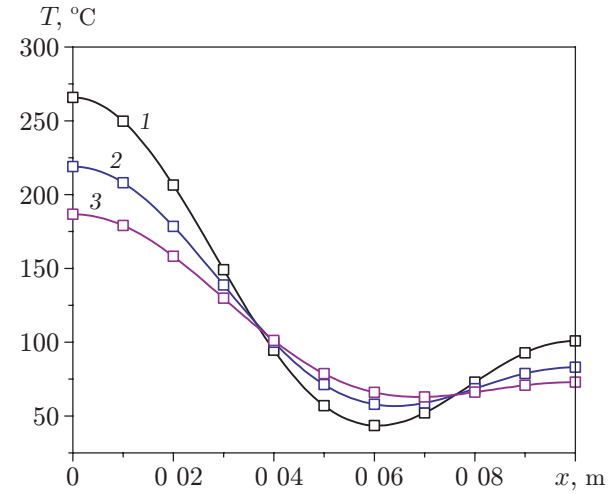

Fig. 6.

Fig. 5. Temperature distributions versus time for various lag times of heating τ: $\tau = 20$ (*1*) and 25 s (*2*).

Fig. 6. Temperature distributions along the plate for various heating times: $t = 10$ (*1*), 20 (*2*), and 30 s (*3*).

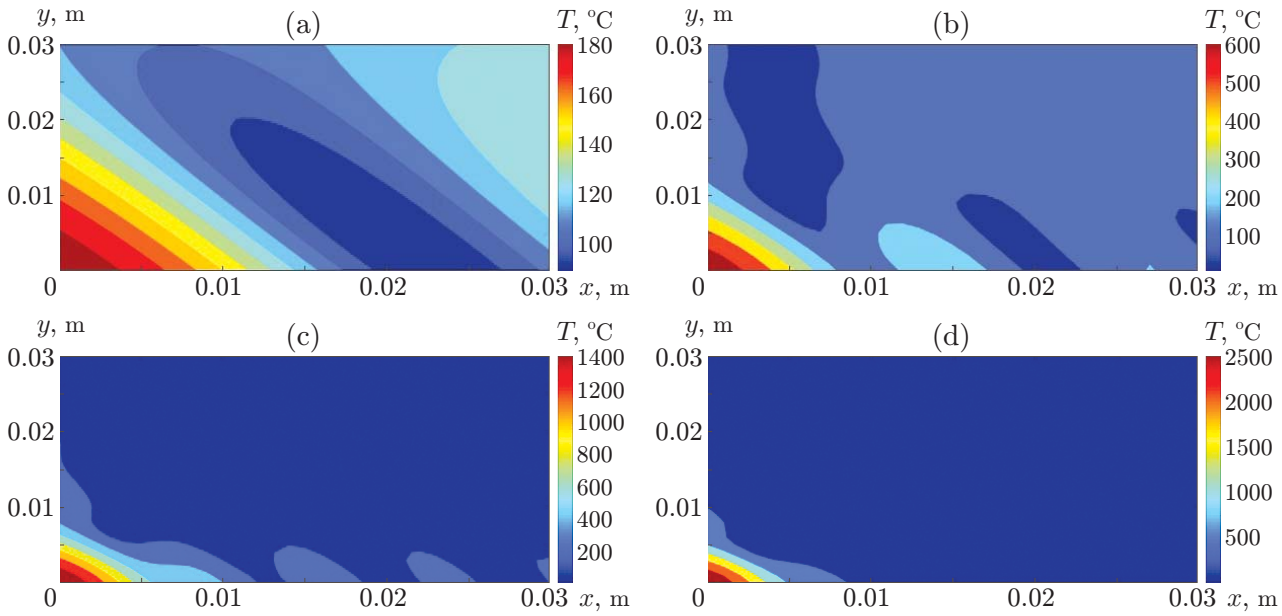

Fig. 7. Temperature distributions for various numbers of finite spatial harmonics N: (a) $N = 5$; (b) $N = 15$, (c) $N = 25$; (d) $N = 35$.

the lag time of heating increases from 10 to 30 s, and the temperature curve $T(x)$ becomes flat gradually (its slope decreases). It also follows from Fig. 6 that the boundary conditions are satisfied at $x = 0$ and $x = 0.1$ m.

As the present mathematical modelling is based on the Fourier transform, the solutions are obtained in both real and complex domains. However, the temperature in the physical domain can be obtained by means of conversion of real temperature from the complex domain by selecting suitable spatial harmonics (see Eq. (14)).

Figure 7 shows the temperature distributions for $v = 0.005$ m/s, $a_f = 0.03$ m, $b = 0.005$ m, $\delta = 0.008$ m, $Q = 25\,000$ W, $f_f = 0.42$, and various numbers of spatial harmonics. It is noticed from Fig. 7 that the heat flow changes depending on the number of spatial harmonics (5, 15, 25, and 35). For $N = 5$ and 15, the difference in the heat flow is observed in the form of thermal contours. However, for $N = 25$ and 35, similarity of the thermal contours with negligible variation is observed. Thus, 35 harmonics are sufficient for adequate modeling of the heat flow by the proposed method.

Figure 8 shows the thermal contours for various times of heating. The peak temperatures obtained in the surface contour plot depict the orientation of energy propagation in the physical domain, and it justifies the concept of rapid heating and gradual cooling as experienced in the submerged arc welding process.

CONCLUSIONS

A method of finding an analytical solution of the heat transfer problem modeling the thermal response captured in the submerged arc welding process is proposed. The research output is successfully validated with existing experimental results. This theoretical study might be a benchmark for deciding the design protocols of submerged arc welding.

CONFLICT OF INTEREST

The author firmly declares the non-existence of this conflict of interests in this research work.

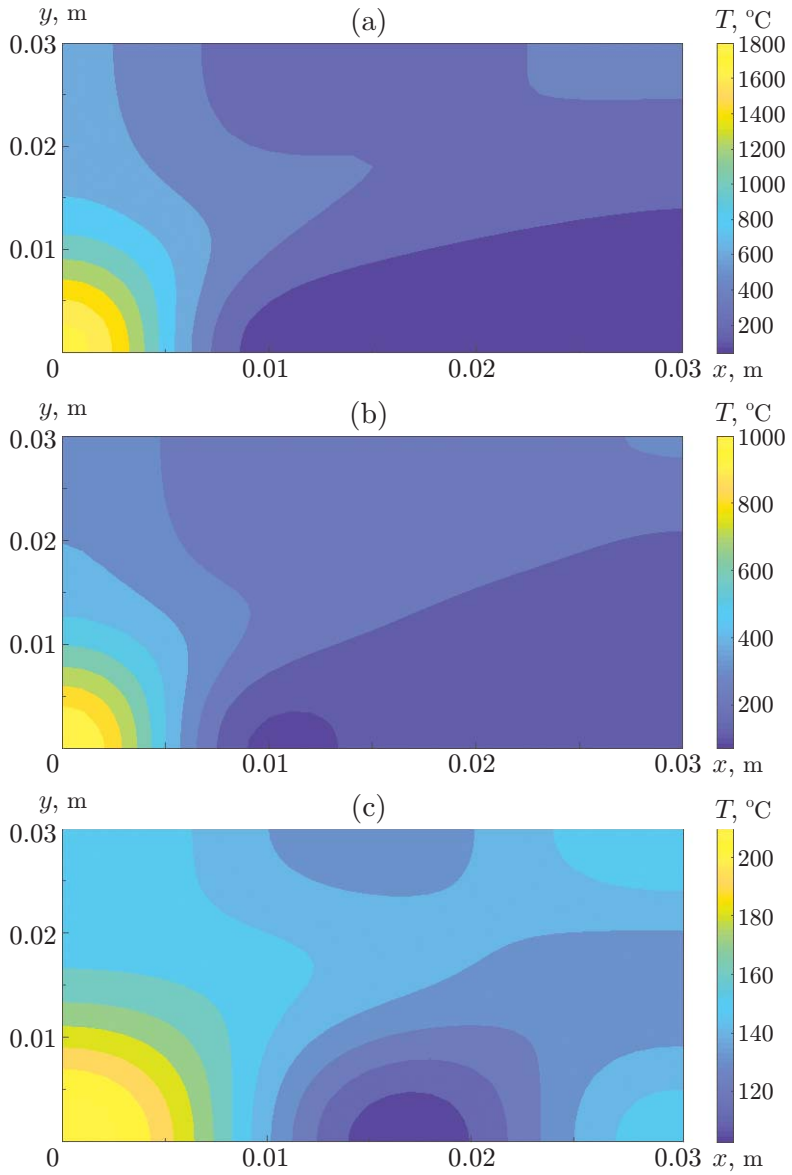

Fig. 8. Thermal contours for various times of heat exposure: (a) $t = 5$ s; (b) $t = 15$ s; (c) $t = 20$ s.

REFERENCES

1. J. R. Davis, *ASM Specialty Handbook Carbon and Alloy Steels* (ASM Intern., 1996).
2. J. Goldak, M. Bibby, J. Moore, et al., "Computer Modelling of Heat Flow in Welds," Metallurg. Trans. B **17**, 587–600 (1986).
3. A. Daemen and F. Dept, "Submerged-Arc Stainless Steel Strip Cladding," Weld. Res. Suppl. 33–40 (1970).
4. P. Biswas, M. M. Mahapatra, and N. R. Mandal, "Numerical and Experimental Study on Prediction of Thermal History and Residual Deformation of Double-Sided Fillet Welding," Proc. Inst. Mech. Engrs. B. J. Engng Manufacture **224**, 125–134 (2009).
5. A. Ghosh, N. Barman, H. Chattopadhyay, and S. Bag, "Modelling of Heat Transfer in Submerged Arc Welding Process," Proc. Inst. Mech. Engrs. B. J. Engng Manufacture **227** (10), 1467–1473 (2013).
6. A. Ghosh and H. Chattopadhyay, "Mathematical Modeling of Moving Heat Source Shape for Submerged Arc Welding Process," Intern. J. Adv. Manufactur. Tech. **69**, 2691–2701 (2013).

7. D. C. Birsan, E. Scutelnicu, and D. Visan, "Modeling of Heat Transfer in Pipeline Steel Joint Performed by Submerged Double-Arc Welding Procedure," Adv. Materials Res. **814**, 33–40 (2013).
8. V. A. Sudnik, V. A. Erofeev, A. V. Maslennikov, et al., "A Mathematical Model of the Submerged-Arc Welding Process and Phenomena in the Arc Cavity," Weld. Intern. **27** (8), 629–637 (2013).
9. D. Podder, N. R. Mandal, and S. Das, "Heat Source Modeling and Analysis of Submerged Arc Welding," Weld. J. **183**, 1–10 (2014).
10. A. Yadav, A. Ghosh, and A. Kumar, "Experimental and Numerical Study of Thermal Field and Weld Bead Characteristics in Submerged Arc Welded Plate," J. Materials Process. Technol. **248**, 262–274 (2017).
11. J. Dutta, N. Mandal, F. Chatterjee, and G. Kibria, "Evaluation of Thermal Characteristics of Laser Induced Heating of Microfilm in Relation to Printed Circuit Board Manufacturing," Proc. Inst. Mech. Engrs. E. J. Proc. Mech. Engng. (2022). DOI: 10.1177/09544089221116165.
12. H. Sharma, B. Rajput, and R. P. Singh, "A Review Paper on Effect of Input Welding Process Parameters on Structure and Properties of Weld in Submerged Arc Welding Process," Materials Today: Proc. **26** (2), 1931–1935 (2020).